HEFAT2007
5th International Conference on Heat Transfer, Fluid Mechanics and Thermodynamics
Sun City, South Africa
Paper number: K6

THE THERMODYNAMICS, HEAT TRANSFER AND FLUID MECHANICS ROLE OF LUBRICANT OIL IN HERMETIC RECIPROCATING COMPRESSORS

A.T. Prata* and J.R. Barbosa Jr.
*Author for correspondence
Department of Mechanical Engineering,
Federal University of Santa Catarina,
Florianopolis, SC, 88040-900,
Brazil,
E-mail: prata@polo.ufsc.br

ABSTRACT

The present paper reviews recent developments on the influence of oil on several thermophysical phenomena in reciprocating compressors. Besides the more essential role of lubrication, the oil is responsible for several tasks in the compressor, from cooling to keeping a low system pressure while the compressor is idle. Thermodynamics dictates the amount of dissolved refrigerant the oil can retain at a particular condition. Hence, the viscosity of the lubricant is directly affected by the refrigerant solubility in the oil. Heat transfer is crucial for keeping a low temperature in the compressor because thermodynamic losses increase with increasing gas temperature. Fluid mechanics is essential to guarantee that oil is delivered to the bearings and that lubrication is performed efficiently under any operating condition.

INTRODUCTION

As with other economic sectors, the refrigeration industry is being faced by many challenges through recent and present times concerning ecological sustainability and environmental impact. CFCs have already been banned in many countries and HCFCs (their temporary replacements in the refrigeration industry) will be so by 2030 in many parts of the developed world [1].

It is widely acknowledged, however, that the issue of Global Warming should not be looked at only from a perspective of direct emissions, i.e., refrigerant leakages during operation and equipment end-of-life. As pointed out by many sources [1-3], approximately 80% or more of the Global Warming impact of refrigeration plants is due to energy consumption (an indirect effect), and not to refrigerant leakage. There are more than 10^9 domestic refrigerators currently in operation worldwide, which corresponds to a doubling of the production between 1990 and 2002 [1]. In worldwide commercial refrigeration, there are more than 75×10^6 units in operation [4]. Overall, refrigeration consumes about 15% of all electricity produced worldwide, and the latter is mostly associated with fossil fuels. Reducing the energy consumption of refrigeration systems has now become a key environmental priority [1].

A typical household refrigeration appliance operates according to the thermodynamic cycle shown in Figure 1. The compressor is responsible for moving the refrigerant through the components of the cycle and for, together with the expansion device, establishing regions of low and high refrigerant saturation pressure in the cycle. The removal of the cooling load from the ambient and its rejection (together with the compressor work, in the form of heat) to the environment is accomplished via the evaporator and condenser, respectively. An internal heat exchanger is often utilized as a means of increasing the refrigeration capacity by admitting a low vapor quality refrigerant in the evaporator [5]. This heat exchanger also guarantees that no liquid is present in the compressor suction by superheating the vapor as it leaves the evaporator. Figure 2 shows a *p-h* diagram of the vapor compression cycle.

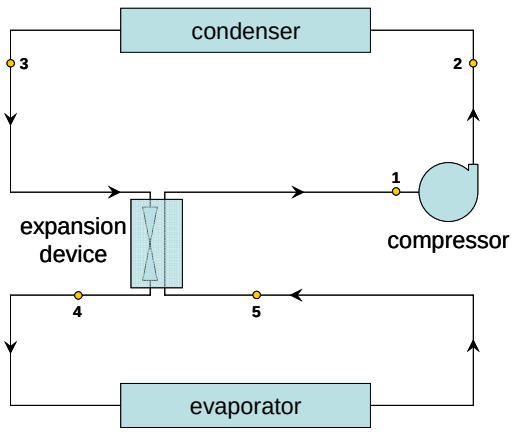

Figure 1 Single-stage (standard) vapor compression cycle

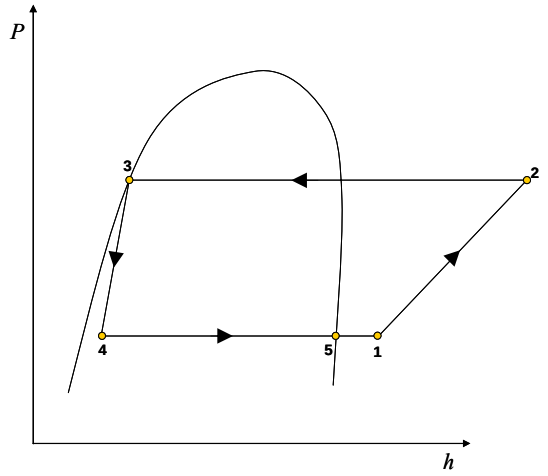

Figure 2 Pressure-enthalpy diagram of a (standard) vapor compression cycle

Reciprocating compressors are widely employed in household and many other applications [3,6,7]. A crank-shaft system driven by an electric motor transforms the rotary motion of the rotor into a reciprocating motion of the piston. In a two-stroke cycle operation, as the piston descends on the suction stroke, the cylinder gas pressure falls until it is lower than the suction line pressure, and the automatic suction valve opens to admit gas from the evaporator. At the bottom of the stroke, this valve closes and the compression stroke begins. When the cylinder pressure is higher than the discharge pressure, the automatic discharge valve opens and the compressed gas passes to the condenser. Clearance gas left at the top of the stroke must re-expand before a fresh charge can enter the cylinder [3].

Losses occur during all stages of the transformation of the electrical energy driving the motor into enthalpy of the refrigerant gas discharged by the compressor. Recent studies [8,9] shed some light on the efficiencies of the energy conversion processes in hermetic reciprocating compressors and characterized the nature of the main losses. Broadly speaking, the energy losses are divided into (i) electrical, (ii) friction, (iii) thermodynamic and (iv) cycle losses. Friction and thermodynamic losses are directly related to the role of oil in a compressor. Friction losses are mechanical losses that take place in the bearings and piston-cylinder gap. Thermodynamic losses involve the flow of refrigerant gas inside the compressor. These are mostly associated with the valve flows (friction and flow reversal), gas leakage through the piston-cylinder gap and refrigerant superheating before (i.e., along the suction path inside the compressor) and during vapor compression [8]. This useless superheating provokes a reduction in volumetric efficiency and refrigerant mass flow rate and an increase in compression work per unit mass [5].

Quoting a fairly recent report issued by the Technical Options Committee of the United Nations Environmental Program (UNEP) on Refrigeration, Air Conditioning and Heat Pumps, Billiard [4] indicated five technological areas where improvements for energy efficiency enhancement are possible, namely, (i) forced convection for evaporators and compressors (ii) lower viscosity oils, (iii) reduction of the temperature level inside compressors, (iv) variable speed motors, and (v) insulation. Of those, items (ii), (iii) and (iv) involve, in a direct way, the role of oil in compressors.

NOMENCLATURE

A	[m^2]	Area
~~a~~	[m^2/s]	Acceleration
~~c~~	[m]	Radial clearance between journal and shaft
~~D~~	[m^2/s]	Diffusion coefficient
$E_{\%}$	[%]	Allowable volumetric heat generation density increase
g	[m/s^2]	Acceleration of gravity
h	[J/kg]	Specific enthalpy, oil film thickness
~~h~~	[W/m^2K]	Heat transfer coefficient
I	[kgm^2]	Inertia tensor
k	[W/mK]	Thermal conductivity
L	[m]	Height of liquid layer
$\dot{m}$	[kg/s]	Mass flow rate
m	[kg]	Mass
N	[-]	Number of droplets
p	[kPa,bar]	Pressure
Pe	[-]	Poynting factor
r	[m]	Radial direction
R	[m]	Droplet radius, Bearing Radius
Ra	[-]	Rayleigh number
$\Re$	[J/kgK]	Gas constant
t	[s]	Time
T	[K]	Temperature
v	[m/s]	Velocity
~~V~~	[m^3]	Volume
x	[-]	Mass fraction (or solubility)
x_R	[-]	Volume-averaged refrigerant mass fraction
z	[m]	Distance

Special characters

α	[rad]	Crankshaft angle
β	[m/s]	Mass transfer coefficient
ε	[-]	Bearing eccentricity ratio
$\dot{\varepsilon}$	[1/s]	Shaft radial velocity
γ	[-]	Activity coefficient
ϕ	[-], [rad]	Fugacity coefficient, connecting rod angle
λ	[m]	Unit length
μ	[kg/ms]	Viscosity
ρ	[kg/m^3]	Density

Subscripts and Superscripts

1,2	Component of the mixture
A	Ambient
b	Bottom
d	discharge
G	Gas or vapour
l	Leakage
L	Liquid
O	Oil
P	Compressor shell
r	Flow reversal
s	Suction
sat	Saturation
x	Along x coordinate
y	Along y coordinate
t	Top
W	Wall

Abbreviations

AB	Alkylbenzene
CFC	Clorofluorocarbon
HCFC	Hydroclorofluorocarbon
MNO	Mineral oil
POE	Polyol ester oil

Besides the main and more obvious role of allowing the moving parts of the compressor to move without wear and with minimum power loss, the lubricant performs many other tasks in the compressor. Among these one may cite cooling, sealing, protecting against corrosion, acting as a hydraulic fluid, reducing the noise level and maintaining low equalizing pressures during the off-cycle.

The ability of the oil to provide adequate lubrication and to be compatible with the refrigerant is crucial for the energy efficiency, reliability and durability. The role of lubrication is intimately related to the lubricant's viscosity. Operating below the minimum or above the maximum viscosity values specified for a particular application may result in wear related malfunction. Using a very low viscosity lubricant gives rise to direct metallic contact between the sliding parts due to reduced load capabilities of the bearings system. Very high viscosity fluids, on the other hand, can lack the necessary flow requirements for successful lubrication and wear can occur due to lubricant starvation in the bearings [10].

The importance of adequately specifying the lubrication fluid is made more serious and complex by the influence of two factors, namely, the variation of oil viscosity with temperature and the dilution of the lubricant by the refrigerant. Overall, oil-refrigerant solubility and miscibility are a function of the physico-chemical relationship between their components at the compressor operating condition (temperature and pressure). However, spatial gradients of temperature and pressure developing inside the compressor may result in a non-uniform refrigerant concentration distribution in the oil that can generate, because of the large difference between pure oil and liquid refrigerant viscosities, significant lubricant viscosity gradients in the compressor.

In household and light commercial refrigeration applications, the most commonly utilized oil-refrigerant pairs (POE-HCFC, MNO-HC ― see Nomenclature for a list of abbreviations) experience significant mutual solubilities, which makes the equilibrium thermodynamics of the oil-refrigerant solution a crucial aspect of lubricant selection for a particular compressor and refrigeration application.

Thermodynamics and heat and mass transfer aspects of the oil-refrigerant combination also have a great impact on the refrigeration system operation at transient conditions. In small capacity systems, the cooling capacity is maintained by a succession of on-off compressor cycles whose frequency depends on thermal load and cold ambient temperature requirements. In each cycle, after the compressor turns off, absorption of vapour refrigerant in the oil layer at the bottom of the shell is initiated. This absorption is one of the processes that determine the equalizing pressure, i.e., the pressure attained by the whole system while the compressor is off. If the equalizing pressure is high at compressor start-up (start of the following on-off cycle), the refrigerant vapour density entering the cylinder through the suction valve is also high. Consequently, because of the larger mass of vapour in the cylinder, the discharge pressure is reached before the piston reaches the top dead centre and is maintained for longer during the extended discharge process. This results in higher pressure forces on the piston and in higher resisting torques to be overcome by the electrical motor. Thus, high refrigerant absorption rates in the oil are desirable since lower equalizing pressure means reduced torque and power required for compressor start-up. On the other hand, at the moment of start-up, as the suction pressure falls from the equalizing pressure towards the steady-state suction pressure value, the refrigerant solubility decreases causing vapour to boil out of the oil. In extreme situations, foam generation in the oil layer may become dangerously excessive to the point of liquid reaching the cylinder suction and posing a risk to the reliable operation of the valve system. In some compressors, to reduce the solution of refrigerant in the oil to an acceptable level, heating devices are commonly fitted to crankcases, and remain in operation whenever the compressor is idle [10].

In the compressor, heat is generated mainly due to compression heat and friction between sliding parts. Another source of heat, but of secondary importance, is the electric motor. In hermetic compressors, the lubricant circulating within the shell acts as a 'heat distributor', absorbing heat in high temperature regions and dissipating it at zones of low temperature. Depending on the lubricant flow pattern in the compressor, its role in compressor cooling may be more or less important and some lubricant flow patterns may be more desirable than others when heat rejection to the external environment is critical.

However, considering the way in which it is conventionally utilized (i.e., as a fluid that circulates within the shell, but does not interact with the refrigerant *during* compression itself) the lubricant, as a heat transfer medium in the reciprocating compressor, is still a small player. As pointed out in [6,10], the oil typically absorbs 5-10% of the heat generated in the compressor. As will be discussed later, a much more effective means of using the oil as a way of lowering the compressor thermal profile is to perform an atomization of the oil in the cylinder during compression. For example, with oil injection in screw compressors, the lubricant absorbs much greater amounts of heat and, by modulating the injection temperature and flow rate, a complete control of the discharge temperature is achieved [6].

The objective of this work is to present some recent results of the research on the role of oil in the thermodynamic, heat and mass transfer and fluid flow processes in compressors carried out at the Department of Mechanical Engineering of the Federal University of Santa Catarina. Firstly, thermodynamic aspects of the oil-refrigerant mixtures will be discussed based on experimental data and modeling results generated for mixtures of oil and natural refrigerants (iso-butane and carbon dioxide). Then, absorption of refrigerant in oil will be addressed experimentally and theoretically.

In certain types of hermetic reciprocating compressors, internal lubricant circulation gives rise to an oil falling film on the inner wall of the compressor shell. The influence of this falling film and of the general oil circulation pattern on compressor heat transfer and overall thermal profile is not yet clearly understood. In the first example of the role of oil in compressor heat transfer, a differential model for the heat transfer between the oil, the compressor shell, the refrigerant

vapor inside the compressor and the external environment is formulated and implemented numerically. The numerical results are validated against experimental data for typical operating conditions and are discussed in the light of the role of oil circulation in promoting or inhibiting heat removal from the compressor. In the second study, atomization of oil in the cylinder *during* compression is investigated experimentally and. Oil atomization promotes a heat transfer surface enhancement which favours heat removal from the vapour. The resulting cooling effect also contributes to lowering the overall thermal profile of the compressor parts and, consequently, the initial compression temperature.

The fluid mechanics role of oil is first exemplified by the way oil is pumped from the bottom part of the compressor shell, where it is accumulated, through the rotation shaft. Cost requirements impose that the oil pump should be simple and efficient and thus, in small reciprocating compressors, use is made of the proper rotation as the driving force to overcome gravity and friction as oil is forced through the helical grove that is machined on the shaft, to feed the shaft bearings. From the top of the shaft oil is then expelled to the internal ambient reaching the upper part of the compressor shell and falling back to the sump in the lower part. To proper design the pump as well as the helical grove, channels and passages for a successful lubrication system, it is required a detailed understanding of the oil flow which is made complex by refrigerant out-gassing as well as gas-liquid interface tracking. Some of those issues will be covered in the present work.

A further role played by the oil fluid mechanics in hermetic compressors is in the lubrication itself, which is the main purpose of having oil in such compressors. A typical compressor bearing system comprises radial and axial bearings that operate relying on pressure build up due to both the edge as well as squeeze film effects, the later being the main mechanism in the piston pin lubrication. Starvation and oil cavitation are always present and should be taken care to avoid undesirable solid contact and wearing. As will be explored in the following sections, a proper design of the bearing system should take into account that all bearings operate coupled, and misalignment and deformation of the parts need to be considered. Furthermore, because of the aforementioned interaction between oil and refrigeration gas, two-phase flow models are needed and will also be addressed here.

THERMODYNAMICS

Equilibrium Thermodynamics

Equilibrium thermodynamics dictates the number of phases present in an oil-refrigerant mixture and their respective concentrations at a given pressure and temperature. Normally, because of the very low vapour pressure of the oil, the vapour phase is comprised almost entirely by refrigerant (at the pressure and temperature ranges encountered in refrigeration applications). The solubility is defined as the equilibrium refrigerant mass fraction in the liquid phase. It influences the ability of the oil in absorbing and desorbing refrigerant during compressor transients and, because the liquid refrigerant is less viscous than the oil, it also establishes the minimum (theoretical) liquid mixture viscosity at a given pressure and temperature.

The literature on phase equilibrium and physical properties of mixtures of oil and HCFC and CFC refrigerants mixtures is abundant and many recent compilations and reviews are available [11-13]. Recently, in the wake of the development of refrigeration systems that employ natural or alternative refrigerants [14], much attention is being given to the experimental and theoretical characterization of phase equilibrium of mixtures of oil and natural refrigerants [15-20].

Marcelino Neto and Barbosa [21,22] conducted experiments to determine simultaneously the solubility, density and viscosity of mixtures of R-600a (isobutane) and R-744 (carbon dioxide) and synthetic lubricants (POE and AB). The experimental facility (Figure 3) is an AISI 316L equilibrium cell (2) containing specified amounts of pure oil and refrigerant. The system temperature is controlled by a thermostatic bath (1) and the equilibrium cell is instrumented for absolute pressure and temperature at three distinct heights to measure the temperatures of the liquid and vapor phases. A gear pump (5) circulates the liquid mixture through the rig. The mixture first flows through a Coriolis mass flow transducer (4) that records flow rate, temperature and density. An oscillating piston viscometer (3) registers temperature and dynamic viscosity of the liquid mixture. The solubility of the mixture is measured gravimetrically using a liquid mixture sample collected in a sampling cylinder (5).

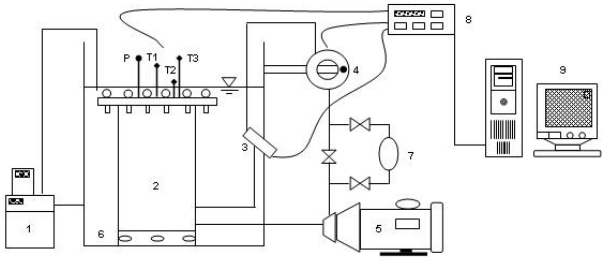

Figure 3 Physical properties experimental rig.

Figure 4 shows a comparison of experimental and predicted bubble point pressure (solubility) as a function of temperature for a mixture of R-600a and POE ISO 7. The solubility is directly proportional to pressure and inversely proportional to temperature. Below the critical temperature of the refrigerant, as the solubility approaches unity, the system pressure tends to the saturation pressure of the pure refrigerant. Equality of component fugacities in the liquid and vapor phases establishes the condition for thermodynamic equilibrium. Thus (assuming that the vapor phase is pure refrigerant), the refrigerant molar solubility is given by

$$\bar{x}_1 = \frac{\phi_1 p}{\gamma_1 p_1^{sat} \phi_1^{sat} Pe} \qquad (1)$$

In Eq. (1), the refrigerant activity coefficient was calculated through a Flory-Huggins [23] model and the agreement with the experimental data is satisfactory (RMS = 0.66%).

Figure 5 shows the viscosity of R-600a/POE ISO 7 as a function of temperature and molar solubility. A significant departure from ideal viscosity behavior is seen for this mixture. The Grunberg and Nissan [24] and Katti and Chaudry [25] models were used to correlate the data (RMS = 2.96% and 2.00%, respectively).

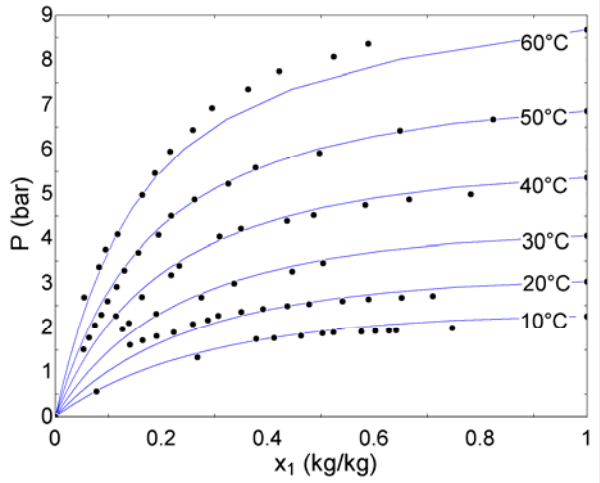

Figure 4 Solubility curve for R-600a/POE ISO 7 [21].

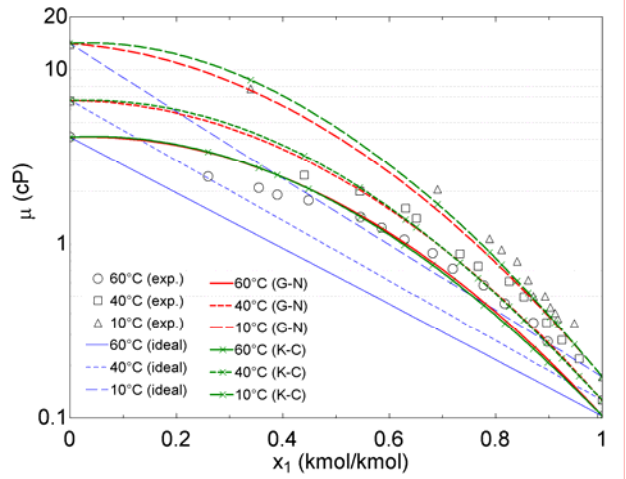

Figure 5 Viscosity of R-600a/POE ISO 7 [21]. G-N = Grunberg and Nissan [24], K-C = Katti and Chaudry [25].

Experimental data for equilibrium pressure as a function of R-744 solubility and temperature are shown in Figure 6 for R-744/POE ISO 68 [22]. At 12 and 25°C, i.e., temperatures lower than the critical temperature of R-744 (30.98°C), the saturation pressure approaches the vapor pressure of the pure refrigerant as the solubility tends to unity. At 25°C, immiscibility and phase separation in the liquid was identified [15]. In this case, for solubilities higher than 0.6, there are three phases in thermodynamic equilibrium: two liquid phases (one with a higher refrigerant concentration and another with a low refrigerant concentration) and one vapor phase.

Absorption and the Path to Equilibrium

As mentioned above, absorption of refrigerant in oil is crucial for the determination of the equalizing pressure in small capacity systems. It depends on oil-refrigerant equilibrium thermodynamics and on heat and mass transport processes in the liquid phase [26-29]. Silva [30,31] conducted a series of experiments to determine the rates of absorption of R-12 in MNO and of R-134 in POE. An absorption cell was constructed so as to measure rates of pressure decay due to refrigerant absorption in a closed system (see Figure 7 for a description of the problem geometry and mechanism of pressure decay). A given amount of pure oil is placed in the test cell (internal volume of 467.14 cm^3 and internal diameter of 100 mm). Upon removal of moisture and non-condensable gases, the oil is brought into contact with refrigerant vapor inside the sealed test cell. As the oil absorbs the refrigerant, the system pressure decreases. Experiments were performed at 15, 20 and 23°C and the initial pressure of the refrigerant was of the order of 300 kPa in all cases.

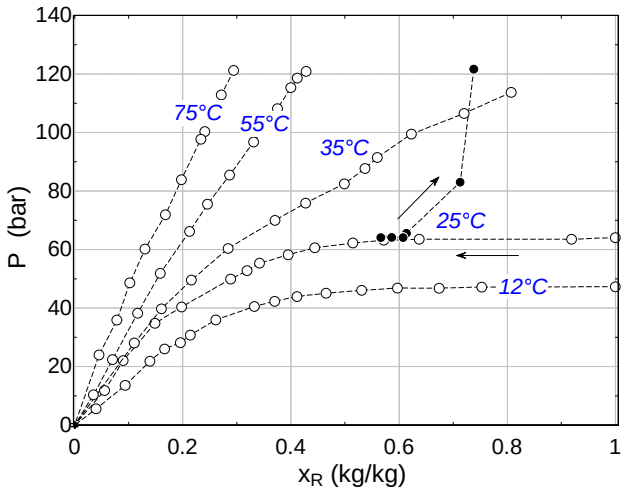

Figure 6 Solubility of R-744/POE ISO 68 [22].

A 2D model based on mass, momentum and species conservation equations for the liquid mixture was proposed by Silva [30] to solve the time-dependent refrigerant absorption taking into account the variation of height of the liquid layer. The governing equations are as follows

$$\frac{\partial \rho_L}{\partial t} + \nabla \cdot (\rho_L \vec{v}) = 0 \qquad (2)$$

$$\rho_L \frac{Dv_z}{Dt} = -\frac{\partial p}{\partial z} + \nabla \cdot (\mu_L \nabla v_z) + \rho g_z \qquad (3)$$

$$\rho_L \frac{Dv_r}{Dt} = -\frac{\partial p}{\partial r} + \nabla \cdot (\mu_L \nabla v_r) \qquad (4)$$

$$\rho_L \frac{Dx}{Dt} = \nabla \cdot (\rho_L \mathcal{D}_L \nabla x) \qquad (5)$$

with the following boundary conditions: (i) symmetry with respect to the centre line, no slip and no penetration at the bottom and sides of the cell and (iii) prescribed liquid velocity (from interfacial mass balance) and thermodynamic equilibrium at the interface. The liquid refrigerant concentration is assumed initially equal to zero.

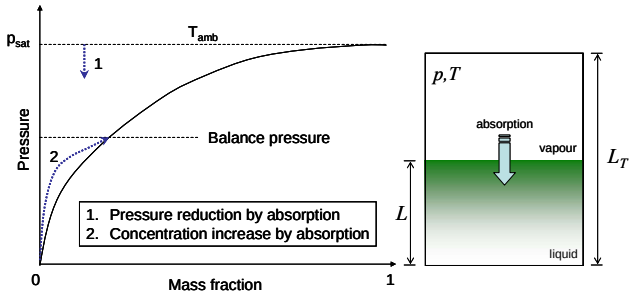

Figure 7 Pictorial representation of the absorption process.

Figure 8 presents curves of pressure decay under constant temperature [30]. The molecular diffusion coefficient is obtained using two different data fitting approaches: (i) a constant diffusion coefficient (blue curves) and (ii) a diffusion coefficient that shows a linear dependence on the local mass fraction (red curves). As can be seen, the general agreement between the experimental data and the calculated profiles is good in both cases, indicating the adequacy of the methodology.

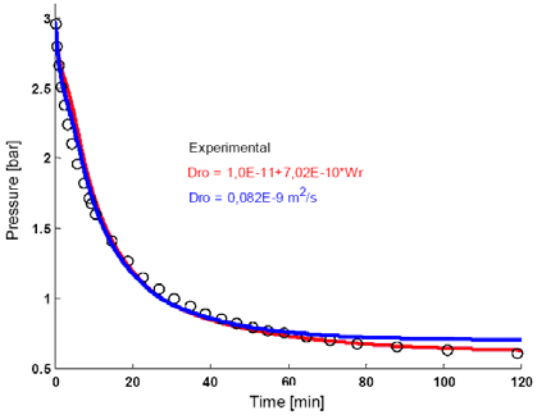

Figure 8 Experimental and calculated pressure as a function of the molecular diffusivity formulation. R134a/POE at 23.4°C [30].

Gessner and Barbosa [32] predicted the absorption of single component refrigerants and refrigerant mixtures in oil through a 1D apparent mass diffusion model. The model was validated with the data of Goswami *et al.* [27] for absorption of R-125, R-32 and R-134a and R-410A (a 50% weight mixture of R-32 and R-125) in POE ISO 68 at pressures ranging from 239 to 584 kPa at 24°C. The diffusion coefficients calculated in [32] for R-125, R-32 and R-134a and oil mixtures were consistent with those obtained by Fukuta *et al.* [29], but one order of magnitude lower than those calculated in [28] (an inconsistency was found in the calculation of the initial depth of the oil layer in [28]). The multicomponent absorption model (R-410A/POE ISO 68) utilized the apparent diffusivity of each oil-refrigerant pair (R-32/POE and R-125/POE) in a matrix method for diffusion of multicomponents [33] under the assumption that interaction effects [34] were not present and the effective apparent diffusivity of each refrigerant (R-32 or R-125) in the liquid mixture was the same as if it were alone in the oil. The 1D multicomponent diffusion equations are given by

$$\frac{\partial}{\partial t}\begin{bmatrix} x_1 \\ x_2 \end{bmatrix} = \begin{bmatrix} \mathcal{D}_{13} & 0 \\ 0 & \mathcal{D}_{23} \end{bmatrix} \frac{\partial^2}{\partial z^2}\begin{bmatrix} x_1 \\ x_2 \end{bmatrix} \tag{6}$$

$$\begin{bmatrix} x_1(z,0) \\ x_2(z,0) \end{bmatrix} = \begin{bmatrix} 0 \\ 0 \end{bmatrix} \tag{7}$$

$$\begin{bmatrix} x_1(0,t) \\ x_2(0,t) \end{bmatrix} = \begin{bmatrix} x_1^I \\ x_2^I \end{bmatrix} \tag{8}$$

$$\frac{\partial}{\partial z}\begin{bmatrix} x_1 \\ x_2 \end{bmatrix}\Bigg|_{z=L} = \begin{bmatrix} 0 \\ 0 \end{bmatrix} \tag{9}$$

The equations were coupled with a semi-infinite diffusion model for the vapour phase and the interfacial mass fractions of the refrigerants were calculated based on the activity coefficient data provided by Burton *et al.* [35] for R-410A/POE ISO 68. Figures 9 and 10 present the predictions of volume average refrigerant mass fraction in the liquid as a function of time for absorption of R-125 and R-410A in POE ISO 68.

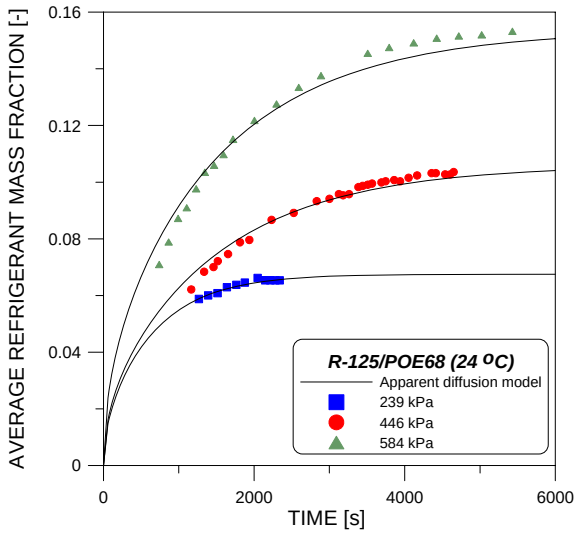

Figure 9 Absorption of R-125 in POE ISO 68 [32].

In an attempt to extend the analysis of Silva [30,31], Barbosa and co-workers [36-38] evaluated experimentally and theoretically absorption of R-134a and R-600a in initially pure POEs for a number of conditions. In addition to pressure, measurements of temperature in both phases and critical time

for the onset of convection in Rayleigh-unstable mixtures were carried out. The latter were performed through visual analysis of video sequences of refrigerant absorption in oil in a transparent test section. A schematic representation of the experimental rig is shown in Figure 11 [38]. Two tests sections were employed in the course of the studies; the main difference between them being the internal diameter of the tube and the number of locations where temperature measurements were carried out. A 150 mm long section made either from a 40 or 70 mm ID borosilicate glass tube is clamped between two aluminum plates. Fittings are screwed on the top plate for connecting pressure (P) and temperature (T) measurement devices and to allow oil and refrigerant charging (C).

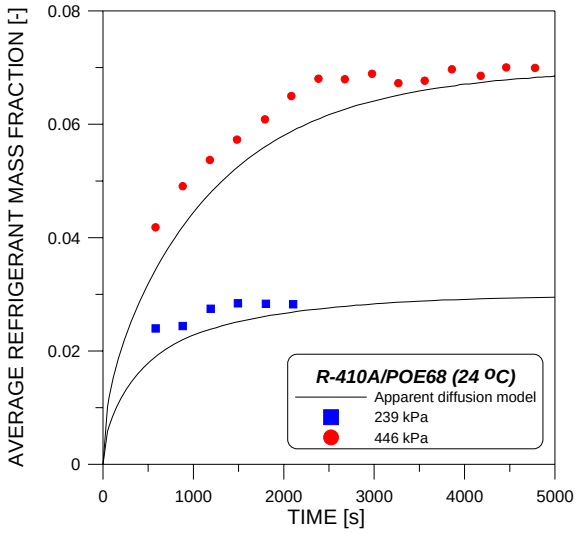

Figure 10 Absorption of R-410A in POE ISO 68 [32].

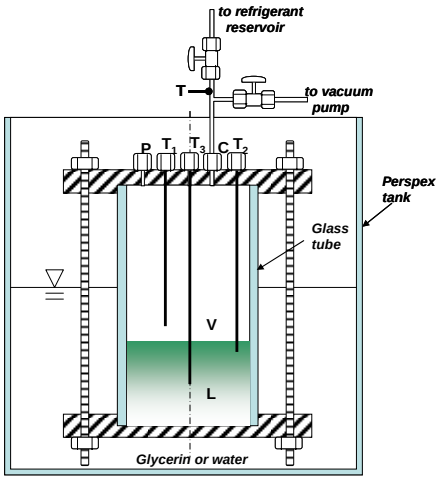

Figure 11 Absorption apparatus [38].

The experimental procedure is similar to that of Silva [30,31] and further details can be found in [37,38]. Two sets of tests were carried out. In the temperature measurement tests, the cell is submerged into a transparent perspex tank filled with circulation water whose temperature is controlled by a thermostatic bath. In the onset of convection visualization tests, the tank is partially filled with glycerin, which has a light refraction index (1.47) very near that of borosilicate glass (approximately 1.5). In addition, any image distortion provoked by the curvature of the glass wall is cancelled out by visual observation of the flow field through the flat walls of the perspex tank. The room temperature was maintained at 25 ± 0.5°C in all tests. Shortly before opening the valve that connects the test section with the refrigerant tank, the computerized data acquisition procedure is initiated.

Figure 12 shows a visualization run for a condition in which the system was maintained at ambient temperature and the initial pressure corresponded to approximately 95% of the saturation pressure of the refrigerant at the ambient temperature. The time elapsed since the first frame is shown for each frame. As can be seen, absorption appears to begin with a disturbance of the interface, just as described qualitatively by Tan and Thorpe [39,40]. The disturbances then evolve into descending inverted plumes that are a typical feature of natural mass convection.

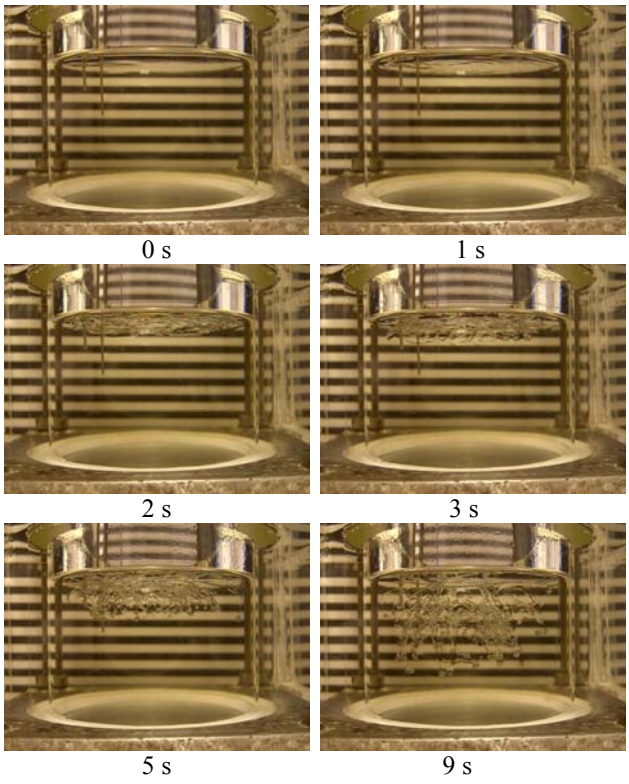

Figure 12 Visualization of absorption of R-134a in POE ISO 10 oil [38].

A simplified model [37] has been put forward to predict the absorption process. Assuming that (i) the vapour behaves as an ideal gas, (ii) the system is isothermal, (iii) the vapour phase is made up only of refrigerant and (iv) the liquid layer height

variation is negligible, mass conservation in the vapour and liquid give

$$\frac{dp}{dt} = -\dot{m}_I \frac{\Re T}{(L_T - L)} \tag{10}$$

$$\frac{dx_R}{dt} = \frac{\dot{m}_I}{\rho_L L}(1 - x_R) \tag{11}$$

The liquid density can be calculated from

$$\frac{d\rho_L}{dt} = \frac{\dot{m}_I}{L} \tag{12}$$

and the interfacial absorption mass flux is modelled in terms of a mass transfer coefficient as follows

$$\dot{m}_I = \beta(x_I - x_R) \tag{13}$$

The mass transfer coefficient is defined in terms of Sherwood and Rayleigh numbers

$$Sh = \frac{L\beta}{\rho_L \mathcal{D}_L} = C\, Ra_L^n = C\left[\frac{(x_I - x_R)\rho_L g L^3}{\mu_L \mathcal{D}_L}\right]^n \tag{14}$$

The interfacial refrigerant mass concentration (solubility), x_I, was calculated using Raoult's law and the average liquid mass diffusivity was assumed equal to 5×10^{-10} m^2/s. Further details about the selection of coefficients for the mass transfer coefficient dependency on the Rayleigh number and the computational implementation for a number of cases involving absorption of R-134a in POE ISO 10 and POE ISO 7 can be found in [37,38].

Figure 13 shows comparisons between experimental data and predictions of the simplified model for absorption of R-134a in POE ISO 10 [37]. The dimensionless pressure is defined as the ratio of the instantaneous pressure to the maximum pressure in the test section. The system temperature was kept constant and the height of the liquid layer was set at 40 mm (1 *D*), 20 mm (0.5 *D*) and 4 mm (0.1 *D*). As expected, higher rates of absorption are sustained for longer as the initial height of the liquid layer increases. This is because a smaller amount of refrigerant is required to saturate the liquid mixture at a small liquid height. As a result, lower pressures are observed for larger liquid heights. In addition, because the refrigerant supply for a particular experimental run is finite, more oil also means less refrigerant mass available in the test cell.

Tan and Thorpe [39,40] developed a theory for the onset of free convection in a liquid layer due to unstable transient heat conduction and mass diffusion. In the latter case, convection commences when a critical Rayleigh number is attained

$$Ra_{cr} = \left.\frac{g z_{max}^4}{\mu_L \mathcal{D}_L}\frac{\partial \rho_L}{\partial z}\right|_{z_{max}} \tag{15}$$

Assuming (i) full miscibility, (ii) ideal liquid density and (iii) average liquid viscosity and diffusivity, the critical depth at which convection initiates is given by $\partial Ra/\partial z = 0$, i.e.,

$$z_{max} = -4\frac{\partial x}{\partial z}\left[\frac{\partial^2 x}{\partial z^2} + 2\rho_L\left(\frac{1}{\rho_O} - \frac{1}{\rho_R}\right)\left(\frac{\partial x}{\partial z}\right)^2\right]^{-1} \tag{16}$$

According to Tan and Thorpe [40], the equivalent transient Biot number for interfacial diffusion determines whether an interface approaches the theoretical limits of Fixed Surface Concentration (FSC) ($Bi_D = \infty$) or Constant Mass Flux (CMF) ($Bi_D = 0$) boundary conditions. As R-134a is very soluble in POEs, a small Bi_D is produced, which corresponds to a CMF boundary condition. It has been shown (see [39,40] for a literature review and extensive discussions) that the value of *Ra* in the theoretical limits of FSC and CMF boundary conditions are 1100 and 669, respectively.

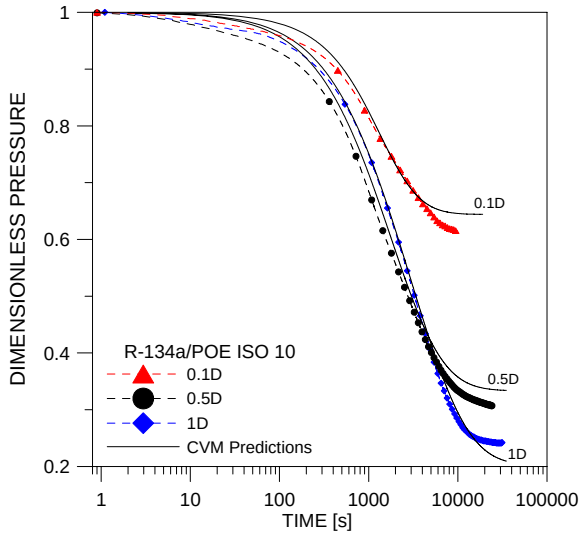

Figure 13 Pressure as a function of time. Effect of liquid layer height [37].

Prior to the onset of convection, the local refrigerant mass fraction is calculated assuming that absorption is due solely to diffusion in a deep fluid (a semi-infinite medium). Thus, by assuming average transport properties and solving the species conservation equation for a constant mass flux boundary condition, one has

$$x(z,t) = x_0 + \frac{2m_I''}{\rho_L}\sqrt{\frac{t}{\mathcal{D}_L}}\,\mathbf{i}\mathrm{erfc}\left(\frac{z}{2\sqrt{\mathcal{D}_L t}}\right) \tag{17}$$

Given that the value of the critical Rayleigh number has been established at approximately 669 for conditions similar to those of R-134a/POE oil, Eq. (15) was utilized to determine the critical time for the onset of convection [38].

Figure 14 shows the calculated critical time for the onset of natural mass convection as a function of system temperature and pressure for absorption of R-134a in POE ISO 10. At a given temperature, the lowest critical time corresponds to the condition where the initial system pressure is equal to the refrigerant saturation pressure. The critical time for the onset of convection increases whenever the mass transfer driving force

(i.e. the difference between the interfacial and bulk refrigerant mass fractions) decreases. This decrease may be due to a reduction of pressure at constant temperature or a temperature increase at a given pressure. Barbosa *et al.* [38] obtained an encouraging agreement between measured and predicted critical times for the onset of convection for absorption of R-134a in POE ISO 7 and ISO 10 at 25 ± 0.5°C at conditions of rapid release of refrigerant from the reservoir into the test cell.

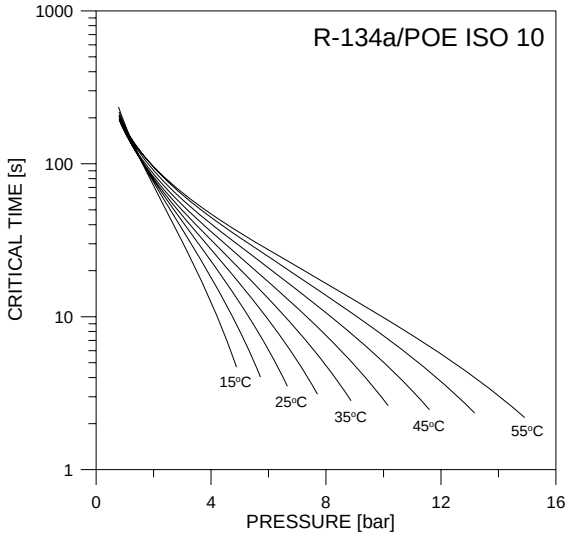

Figure 14 Predictions of critical time for the onset of convection [38].

HEAT TRANSFER

A Model for the Oil Heat Transfer

Pizarro-Recabarren et al. [41] carried out experiments and developed a differential model to evaluate the role of lubricant oil circulation inside the compressor on heat transfer. It is assumed that the oil film on the inner wall of the compressor is laminar and hydrodynamically fully developed. With respect to a coordinate *s* along the oil flow on the shell wall (along points 1 to 6 in Figure 15), the energy balances for the oil and compressor shell are given by

$$\dot{m}_O c_{pO} \frac{dT_O}{ds} = \frac{k_O A}{s} \frac{d}{ds}\left(s \frac{dT_O}{ds} \right) + \hbar_{GO} \lambda (T_G - T_O) + \hbar_{OP} \lambda (T_P - T_O) \quad (18)$$

$$0 = \frac{k_P A}{s} \frac{d}{ds}\left(s \frac{dT_P}{ds} \right) + \hbar_{PA} \lambda (T_A - T_P) + \hbar_{OP} \lambda (T_O - T_P) \quad (19)$$

The heat transfer coefficient between the oil and inner shell wall, $\hbar_{OP}$, was determined based on semi-empirical correlations or CFD simulations of the oil flow in specific regions of the compressor (for example, the zone of oil jet impingement at the top of the shell, the falling film region on the side wall and the carter). The heat transfer coefficient between the outer shell wall and the surrounding air, $\hbar_{PA}$, was determined from standard mixed convection correlations for the Nusselt number assuming that the compressor is approximately spherical in shape [42]. The heat transfer coefficient between the oil, $\hbar_{GO}$, and the internal refrigerant vapour is estimated based on experimental data and a model for the overall heat balance in a compressor [43].

A compressor was instrumented for temperature measurements at ten locations on several parts of its shell more measurements were performed on some internal pieces. Figure 15 presents a comparison between the model predictions and average temperature data on six points along the outer wall of the compressor shell.

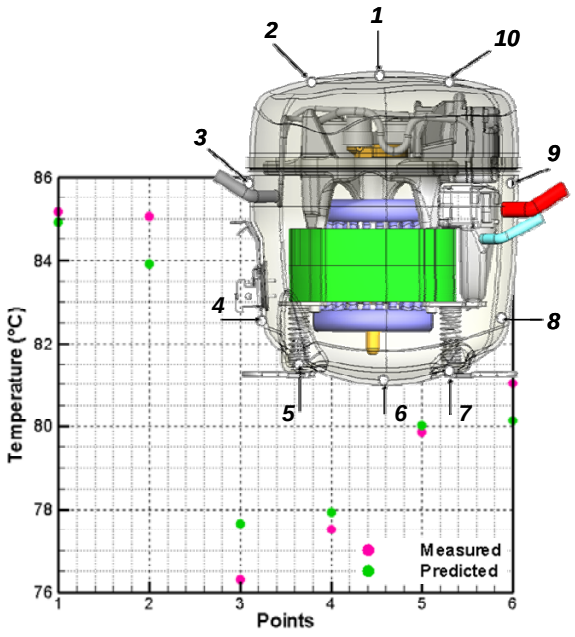

Figure 15 Temperature measurements and predictions on a compressor shell [41].

Agreement between experimental data and model results were satisfactory at two operating conditions. As far as the heat transfer in the compressor is concerned, the role of falling film oil flow on the inner wall is to inhibit heat dissipation from the compressor to the external ambient. It was found that if the film mass flow rate is increased by 20%, the average compressor thermal profile increases by 2 to 2.5°C.

Oil Atomization during Compression

Kremer [44,45] conducted experiments and formulated a differential model to investigate the heat transfer between oil droplets atomized into the cylinder of a reciprocating compressor and the refrigerant gas (R-134a). Oil atomization promotes a heat transfer surface enhancement which favours heat removal from the vapour. The resulting cooling effect also contributes to lowering the overall thermal profile of the compressor parts and, consequently, the initial compression temperature (thereby reducing the thermodynamic losses).

The control volume formulation of the vapour compression process is based on the work of Ussyk [46]. The mass and energy conservation equations for the vapour in the cylinder are given by

$$\frac{dm}{dt} = \sum \dot{m} = \dot{m}_s - \dot{m}_d - \dot{m}_l - \dot{m}_{sr} + \dot{m}_{dr} \tag{20}$$

$$m\frac{du}{dt} = \dot{Q}_o + \hbar A_w\left(T_w - T\right) - p\frac{d\forall}{dt} - u\frac{dm}{dt} - \sum \dot{m}h \tag{21}$$

where $u = u(p,T)$ is the internal energy of the vapour and

$$p = \frac{m}{\forall} Z\Re T \tag{22}$$

$$\sum \dot{m}h = \left(\dot{m}_d + \dot{m}_l + \dot{m}_{sr}\right)h - \dot{m}_s h_{sc} - \dot{m}_{dr} h_{dc} \tag{23}$$

The compression cycle is divided into n time steps of size Δt. The number of spherical droplets injected into the cylinder in a given time step is given by

$$N = \frac{3\dot{V}_o \Delta t}{4\pi R^3} \tag{24}$$

In the following analysis, the subscripts m,n (as in $N_{m,n}$) denote the group of droplets that were injected into the cylinder at a given instant m and still are in the cylinder at an instant $n > m$. It is assumed that all droplets in each group m are identical with respect to their size, velocity and temperature. If coalescence, break-up and evaporation are neglected, mass and energy conservation for each group m give

$$\frac{dN_{m,n}}{dt} = -\frac{\dot{M}_{m,n}}{M_m} \tag{25}$$

$$\frac{dT_{m,n}}{dt} = \frac{3\hbar_{m,n}}{\rho_o c_{po} R_m}\left(T - T_{m,n}\right) \tag{26}$$

Due to the presence of droplets in the cylinder, a correction is applied to the instantaneous cylinder volume to obtain the volume of vapour

$$\forall = \forall_c - \frac{4\pi}{3}\sum_{m=0}^{n} N_{m,n} R_m^3 \tag{27}$$

$$\frac{d\forall}{dt} = \frac{d\forall_c}{dt} - \frac{4\pi}{3}\sum_{m=0}^{n} R_m^3 \frac{dN_{m,n}}{dt} \tag{28}$$

where $\forall_c$ and its time derivative are calculated from algebraic relationships for the piston position and velocity as a function of the crankshaft angle [46]. The heat transfer rate between all oil droplets and the vapour is given by

$$\dot{Q}_o = 4\pi R_m^2 \sum_{m=0}^{n} N_{m,n}\hbar_{m,n}\left(T_{m,n} - T\right) \tag{29}$$

Valve displacement during suction and discharge is calculated via a one-degree-of-freedom model with natural frequency and damping coefficients specific for each valve.

In order to provide the in-cylinder vapour compression and droplet heat transfer models with appropriate boundary conditions, the methodology was incorporated into an existing lumped heat transfer (overall thermal conductance) model that integrates several compressor components [43]. In the original model (without oil atomization), the compressor was divided into eight control volumes (the vapour in the suction muffler, the cylinder walls, the vapour in the discharge muffler, the vapour in the discharge line, the vapour in the compressor shell, the compressor shell, the electric motor and the radial bearings). Steady-sate energy balance equations were written for each component and solved coupled with the transient in-cylinder vapour compression equations. Kremer *et al.* [45] extended the model so as to include another control volume (the oil injection line) and to account for the flow of oil through the components downstream of the cylinder.

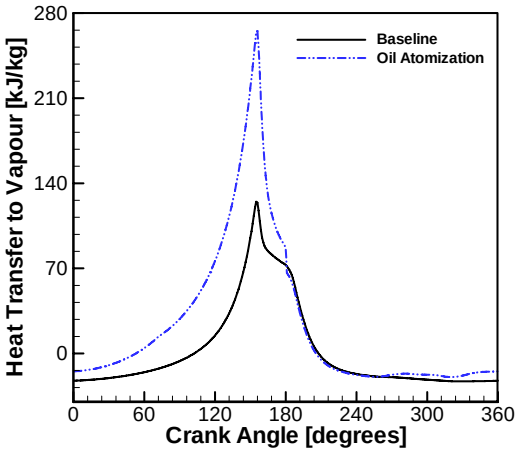

Figure 16 Heat transfer as a function of crank angle [45].

The conditions simulated in [45] were as follows: (i) evaporation and condensation pressures: -27°C and 42°C (R-134a); (ii) vapor temperature entering the compressor (suction line): 32°C; (iii) compressor speed: 60Hz; (iv) piston diameter and stroke: 22.5 and 19 mm; (v), clearance volume: 300 mm^3. For the baseline case (without oil injection), the calculated refrigerant mass flow rate, refrigeration capacity and thermodynamic ($p\forall$) compression power were 3.50 kg/h, 180.8 W and 76.56 W ($COP_{p\forall}$ = 2.36), respectively.

Figure 16 shows the transfer of heat from the vapor as a function of the crank angle for atomization of oil at 45°C, with an average flow rate of 0.916 kg/h. In the atomization case, heat transfer during compression increases more sharply and becomes positive earlier in the cycle showing a strong influence of droplet heat transfer. During expansion, heat transfer is similar in both cases (with and without oil) as a result of the very low velocity of the droplets remaining in the clearance volume after discharge. In Figure 17, *TV* diagrams reveal a significant reduction of the vapor temperature (maximum of 25°C at the top dead centre, TDB). The initial compression

temperature decreases from 58.8 to 44.6°C, illustrating the large potential for reducing losses due to refrigerant superheating.

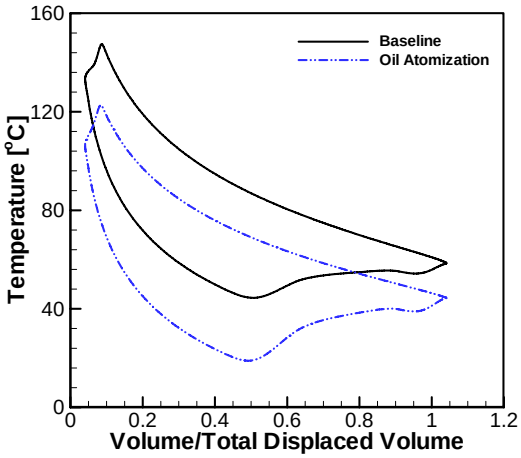

Figure 17 *TV* behavior of refrigerant vapor [45].

FLUID MECHANICS

Oil Pumping

Only recently the oil pumping problem in hermetic compressor has been receiving more attention in the literature [47-52]. Those researches have been motivated by the increasing demand for more efficient lubrication system to reduce energy consumption and improve reliability. Previous experimental work [53-55] treated the problem with less emphasis on more elaborated physical and mathematical models relying on experiments and empirical models. Lückmann *et al.* [52] were the first to perform a detailed analysis of oil pumping in reciprocating compressors. Those compressors usually have a centrifugal pump operated with a reed on its inlet. The reed is placed with an angle that, under rotation, provides the driving force for pumping the oil. Of particular interest is the time required for the oil to reach the bearings once the compressor is started. Void fractions representing the oil interface at the compressor start up is presented in Figure 18. Good design need to avoid irregular passages where pressure drops can lead to out gassing from the oil increasing the pumping time as well as precluding a regular lubricant flow through the bearings.

Others types of pump have been investigated for using in hermetic compressor. Example include the helical screw pump [52,56]. Results for the oil flow rate during the start up period of such pumps are presented in Figure 19. As seen from the figure it takes approximately 0.8 s for the oil to reach the shaft inlet. During this period of time the shaft bearings operate with limited or no oil. Even after the oil starts to flow along the shaft grove, it takes around three seconds to stabilize the oil supply.

Numerical simulations of the oil pumping require great computer time due to the complexity of both the problem geometry and the mathematical model. In this regard Alves *et al.* [56] developed simplified models that could predict the steady state oil flow rate as well as the required time for reaching the steady state. Simple models that make use of fully developed flow assumptions together with some ingenuity were successful in predicting the steady state within 10% deviation from the detailed numerical simulations.

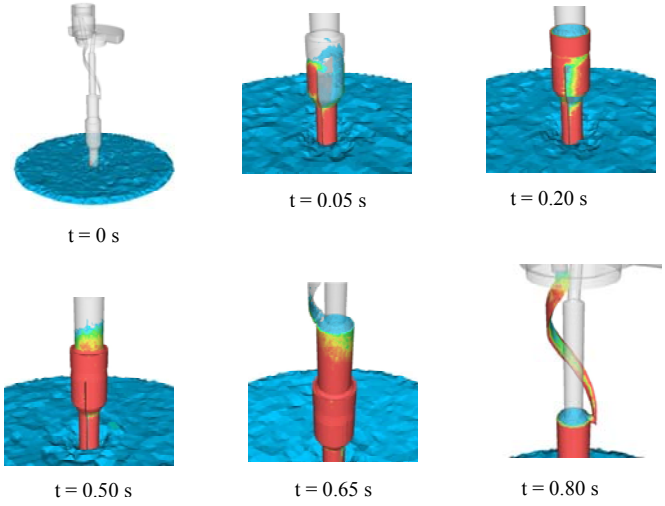

Figure 18 Oil interface (void fractions) at compressor start up for a centrifugal pump operated with reed [52].

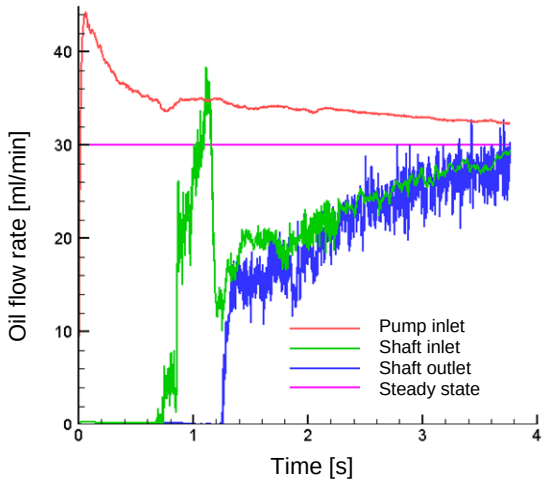

Figure 19 Time evolution of the oil flow during star up for a helical screw pump [52].

Lubrication

A schematic view of a small ringless hermetic reciprocating compressors employed in household refrigeration is depicted in Figure 20, taken form [57]. The system, weighing approximately 1.2 kilograms, is supported by an axial bearing as indicated in the figure. In those compressors the main and sub bearings play a crucial role in maintaining the shaft in its upright position as it rotates, because of the high loads which occur during compression of the gas inside the cylinder. In addition to the shaft and the crankshaft bearings which allow rotation with reduced friction, the axial movement of the piston inside the cylinder bore also requires a proper lubrication. Due

to the dynamics of converting rotation into a primary reciprocating axial movement of the piston, secondary and tertiary radial and oscillatory motions are also present and should be properly accounted for in a detailed analysis of the compression mechanism.

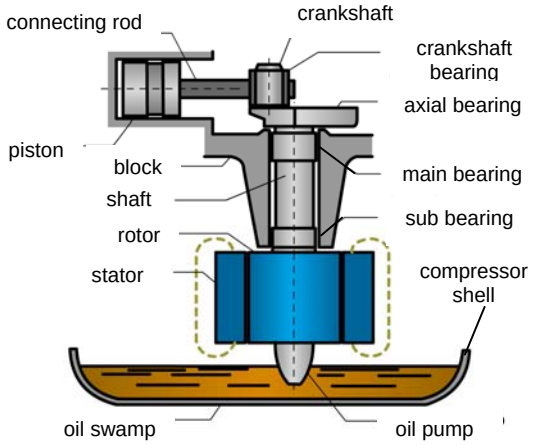

Figure 20 Schematic view of the reciprocating mechanism in a hermetic compressor [57].

In most of the reports available in the literature, the analyses of bearing systems in reciprocating hermetic compressors are performed considering each bearing separately. The axial and radial bearings are usually designed considering the load carrying capacity together with the well established methodology based on the solution of the lubrication equation [58,59]. Piston analysis solutions have also been reported for the secondary piston motion [60-64]. However, very few works consider that the bearings are interconnected and that the system dynamics should be considered incorporating the bearing performances operating together [63]. A complete integral analysis and simulation of the bearing system in reciprocating hermetic compressor was performed for the first time by Huang *et al.* [57], where the influence of each bearing on the dynamics of the system was explored.

The first step in analyzing the lubrication is to explore the kinematics and the dynamics of the compression mechanism. According to Figure 21, the instantaneous piston location can be expressed as

$$\vec{r}_{OB} = \vec{r}_{OA} + \vec{r}_{AB} \tag{30}$$

Furthermore, also from Figure 21 it follows that

$$\vec{r}_{OA} = \overline{OA}(\sin\alpha\hat{i} + \cos\alpha\hat{j}) \tag{31}$$

$$\vec{r}_{AB} = \overline{AB}(-\sin\phi\hat{i} + \cos\phi\hat{j}) \tag{32}$$

where α is the crankshaft angle and ϕ is the connecting rod angle. From Eqs. (30) to (32) it then follows that

$$y_p = \overline{OA}\cos\alpha + \sqrt{AB^2 - (\overline{OA}\sin\alpha + d)^2} \tag{33}$$

where y_p is the piston position along the y-axis and d is the eccentricity between shaft and cylinder axis. From the piston location y_p, the piston velocity and acceleration can be determined taken the first and second time derivative of Eq. (33). Following the same procedure, the kinematics of the connecting rod can be obtained.

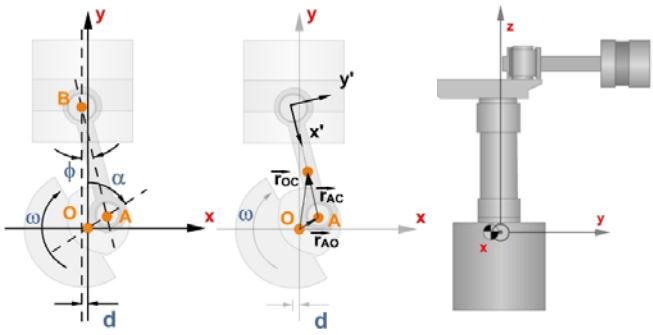

Figure 21 Coordinate systems and nomenclature [57].

The dynamics of each element (piston, connecting rod and shaft) can be resolved from their respective free body diagram, shown in Figures 22 and 23.

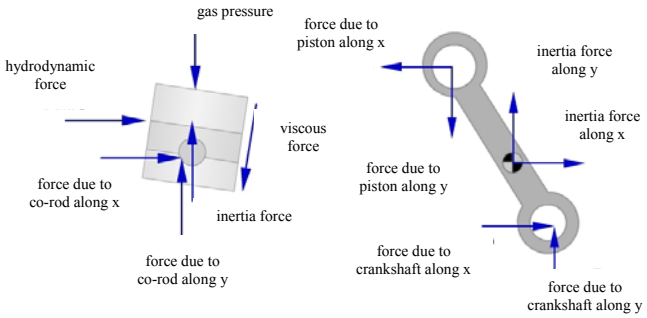

Figure 22 Free body diagrams for piston and connecting rod [57].

Once all the forces acting on each element have been defined, force and moment balances can be performed

$$\sum \vec{F}_{body} = m\vec{a} \tag{34}$$

$$\sum \vec{M}_{body} = \frac{d}{dt}(\bar{\bar{I}} \cdot \vec{\omega}) + \vec{\omega} \times (\bar{\bar{I}} \cdot \vec{\omega}) \tag{35}$$

From the free body diagram for the piston, knowing the gas pressure as a function of time (or as function of the crankshaft angle) it is possible to determine the piston force acting on the connecting rod (which is equal in magnitude and contrary in orientation of the connecting rod force acting on the piston). The gas pressure is usually determined either from experimental measurements or from a thermodynamics analysis of the compressor [46]. Next, a force balance on the connecting rod is performed and from that the force on the crankshaft due to the connecting rod is determined. The last element to be

explored is the shaft, and performing a force and momentum balance on it the applied load on both the main and the sub bearing can be obtained. Those forces are then employed in conjunction with the lubrication equations to calculate the shaft orbit within the bearings. It should be observed that, strictly speaking, the shaft orbit within the bearings affect the system dynamics and because of that both the applied load on the shaft bearings and the lubrication problem should be solved coupled. However, much simplicity is gain with little effect on the results when the dynamics are decoupled from the lubrication problem.

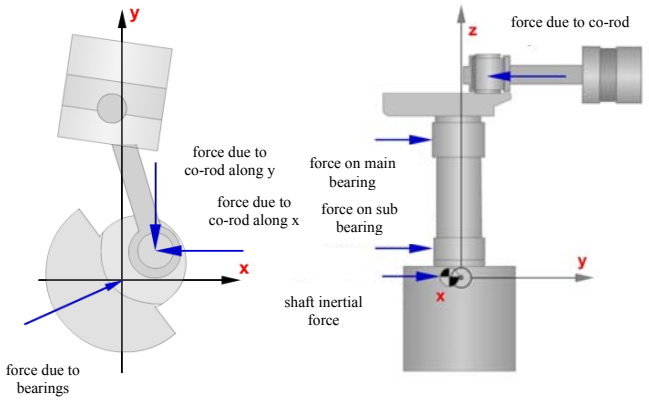

Figure 23 Free body diagrams for shaft on x-y plane and y-z plane [57].

To proper determine the hydrodynamic force which is build up at each bearing to counteract the imposed load use is made of the Reynolds lubrication equation which can be written as [58],

$$\frac{1}{R^2}\frac{\partial}{\partial\theta}\left(\frac{h^3}{6\mu}\frac{\partial p}{\partial\theta}\right)+\frac{\partial}{\partial z}\left(\frac{h^3}{6\mu}\frac{\partial p}{\partial z}\right)=\frac{(U_1-U_2)}{R}\frac{\partial h}{\partial\theta}+ +(V_1-V_2)\frac{\partial h}{\partial z}+2\frac{\partial h}{\partial t} \tag{36}$$

where h is the instantaneous local oil film thickness, U_1 and U_2 are the circumferential journal and bearing velocities, respectively, V_1 and V_2 are the axial journal and bearing velocities, respectively, and θ and z are the circumferential and axial coordinates, respectively. Eq. (36) needs to be integrated along the circumferential and axial directions to determine the local pressure distribution in the oil film. From the integration of this pressure field at each instant of time the hydrodynamic force can be obtained.

From geometrical considerations the instantaneous local oil film thickness, h, can be expressed as

$$h(z,\theta)=c-c[\varepsilon_{tx}+(\varepsilon_{bx}-\varepsilon_{tx})\frac{z}{L}]\cos\theta+ -c[\varepsilon_{ty}+(\varepsilon_{by}-\varepsilon_{ty})\frac{z}{L}]\sin\theta \tag{37}$$

where c is the radial clearance between journal and shaft, ε_{tx} and ε_{ty} are the x and y components of the shaft eccentricity ratio at the top of the bearing, ε_{bx} and ε_{by} are the the x and y components of the shaft eccentricity ratio at the bottom of the bearing, z and θ are the axial and circumferential coordinates along the oil film, respectively, and L is the bearing length. From Eq. (37) the relative radial velocity between journal and bearing, which yields the squeeze film lubrication effect, can be obtained as,

$$\frac{\partial h}{\partial t}=-c[\dot{\varepsilon}_{tx}+(\dot{\varepsilon}_{bx}-\dot{\varepsilon}_{tx})\frac{z}{L}]\cos\theta - c[\dot{\varepsilon}_{ty}+(\dot{\varepsilon}_{by}-\dot{\varepsilon}_{ty})\frac{z}{L}]\sin\theta \tag{38}$$

Equation (36) applies to each bearing and proper account has to be taken for the circumferential and axial velocities, U and V, respectively, depending on the bearing under consideration. For instance, for the lubrication film between piston and cylinder, $U_1=U_2=V_2=0$ and $V_1=V_{piston}$.

As a first approximation with reasonable to good results, for all situations explored oil cavitation can be ignored and the lubricant film can be considered to span from θ=0 to π, in accordance to the well established Gümbel boundary condition [59]. Furthermore, to calculate the shaft orbit, inertia is neglected and it is imposed that at each instant of time the relative radial velocity between journal and bearing, ∂h/∂t, is such that the hydrodynamic force balances the applied load. From that the x and y components of the shaft radial velocity at the top and bottom sides of the bearing can be determined and, in turn, knowing the shaft location at a given time, the shaft location at an increment of time can be obtained as,

$$\varepsilon^{t+\Delta t}=\varepsilon^{t}+\dot{\varepsilon}^{t}\Delta t \tag{10}$$

The numerical solution of the bearing system consists of determining all bearing-shaft orbits in a periodic regime of the reciprocating compressor. To perform a numerical solution for an entire cycle of the crankshaft system encompassing both suction and discharge strokes, the computation starts at a given crankshaft angle (zero, for example) with all eccentricity ratios between journal and bearings equal to zero and proceeds advancing in time until a periodic regime is established. For radial bearings a periodic regime is usually reached after two to three cycles, whereas for the piston between twenty to thirty cycles are required for the periodic regime [57,61,63].

Pressure distributions in the oil film for each bearing that comprises the lubrication system for a typical small size reciprocating hermetic compressor used in household applications are depicted in Figure 24. In those compressors loads of the order of 103 N are applied on the bearings that operate at eccentricity ratios close to 0.9. Figure 25 explores the influence of shaft misalignment on the performance of the crankshaft bearing. As observed in the figure, when shaft misalignment is considered the bearing runs in a more critical situation. The high eccentricities observed on the first quadrant occur on the final stages of the compression cycle and are close to unity, indicating that solid contact between shaft and bearing could happens. Such small eccentricities require that shaft

orbits need to be carefully determined to avoid metallic contact and wear.

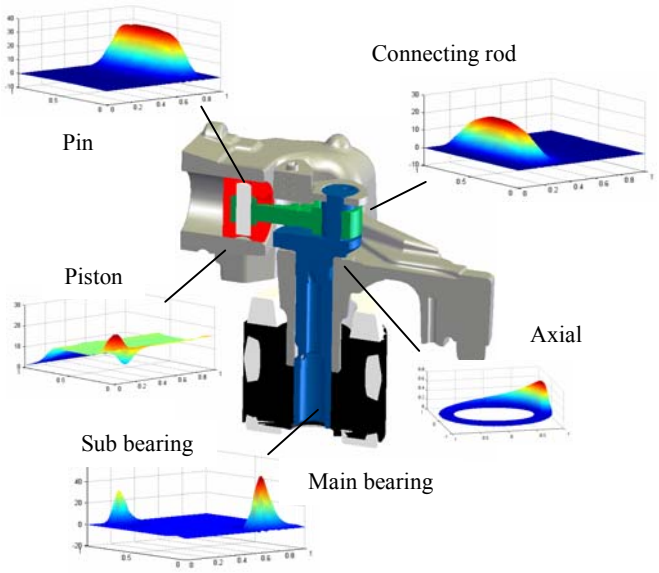

Figure 24 Pressure distributions on compressor bearings [67].

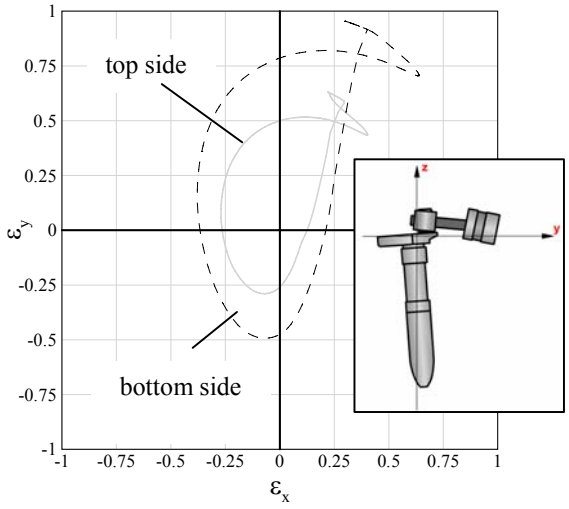

Figure 25 Shaft orbit inside crankshaft bearing; exaggerated picture of misalignment shown in detailed view [57].

Tertiary radial motions of the piston are caused by connecting rod and crankshaft misalignments, weight of piston and connecting rod, and viscous forces. Each one of those moments is presented in Figure 26 as a function of the crankshaft angular position. Because of its small magnitude (less than 10^{-4} N.m) the moment due to the crankshaft misalignment was not plotted. As observed from the figure, the connecting rod moment is more than one order of magnitude larger than the other moments. Those moments act along the y-z plane of the piston (see Figure 21) and may also cause deformation of the connecting rod.

Because of the very small distance between piston an valve plate at the end of the compression stroke, deformations due to both force and moment acting on the connecting rod play an important role and should not be ignored [66].

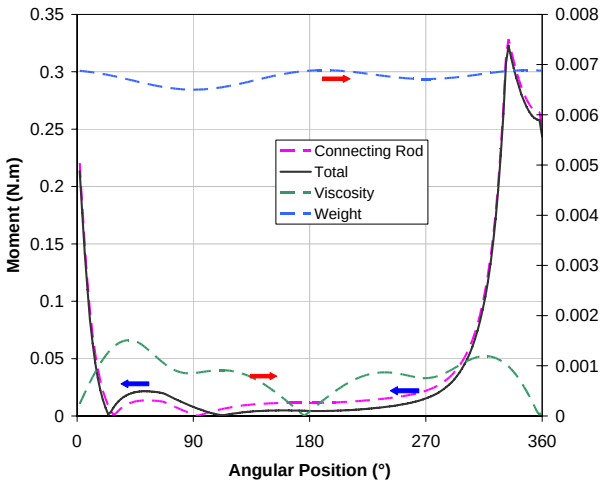

Figure 26 Moments acting on the piston [66].

Two-phase Flow and Cavitation

Disruption of the continuous lubricant film, defined as cavitation, is very common in convergent-divergent geometries such as found in journal bearings [68]. Because of the dilution of the lubricant by the refrigerant, in the divergent region of the bearing the decrease in pressure causes out gassing from the oil and breaks the continuity of the liquid film leading to cavitation. A pictorial representation of gas release and cavitation in bearings is presented in Figure 27. Detailed discussions on the most common conditions in which cavitation occurs can be found in [69].

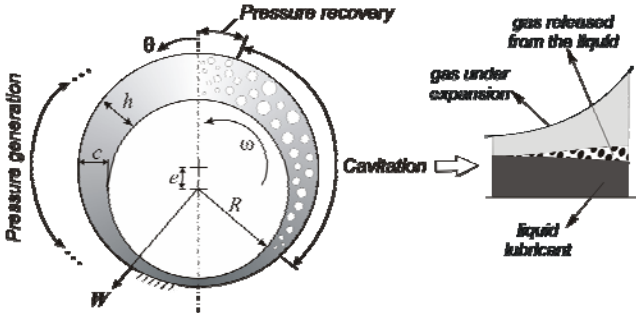

Figure 26 Gas release and film expansion in the cavitated region [68].

Grando *et al.* [68] have recently proposed a homogeneous two-phase flow approach to evaluate the performance of journal bearings under cavitation. The model considered cavitation through out-gassing from an oil-refrigerant mixture under saturation conditions, and no intermediate boundary conditions were required in solving the lubrication equation.

Additionally, a region of pressure recovery was automatically identified near the convergent region of the radial gap. The absorption of refrigerant that can occur under positive pressure gradient was studied under equilibrium and non-equilibrium thermodynamic conditions. Figure 27 presents steady-state pressure results obtained from the classical Reynolds equation as well as from the two-phase flow methodology assuming both equilibrium and non-equilibrium.

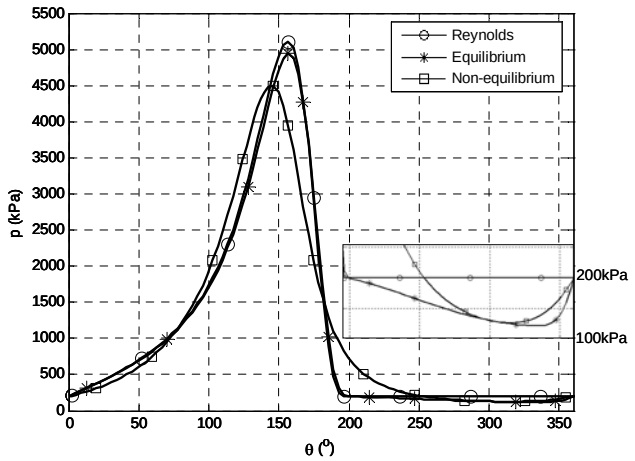

Figure 27 Steady-state pressure results in radial journal bearings in presence of cavitation [68].

For moderate loaded bearing under equilibrium conditions, the two-phase flow model agrees well with the results provided by the classical solution. In those case, only liquid will be present in the convergent region of the fluid film and in this case cavitation can be seen as geometrically determined. In the cavitated region viscosity does not have an important role. Under non-equilibrium conditions, the bearing performance is significantly altered. Gas is present along all the fluid film and its compressibility improves the accommodation of geometry changes. In turn, pressure profile spreads across a wider extent of the bearing and a given load can be supported with lower eccentricity when compared to the equilibrium condition, potentially reducing friction. The two conditions explored, equilibrium and non-equilibrium, represent two limit thermodynamic situations and the actual behaviour of the fluid film will depend on the real rate of absorption of gas by the oil.

The two-phase flow model was applied for investigating the piston dynamics of a small ringless reciprocating compressor [65]. The model predicted power consumption similarly to the single-phase model considering oil-refrigerant viscosity. However, using cavitation criteria as is a common practice, a much lower value was predicted.

CONCLUSIONS

In general, hermetic reciprocating compressors use oil as the lubricant media. However, the importance of the oil extends well over its lubrication expectations. Absorption of refrigeration gas by lubricating oil plays a crucial role in the compressor performance and thus the thermodynamics and thermophysics properties of the oil-refrigerant mixture are very important for compressor design and performance. Oil can also be employed as a heat transfer media both externally and internally in the refrigerant circuitry. Even as lubricant, detailed aspects of how oil is pumped through the bearings and how the bearings themselves performed during their coupled dynamics are essential when accurate designs are sought. All those issues were addressed and reviewed in the present contribution.

ACKNOWLEDGEMENTS

The work reported here has been made possible through financial support from CNPq, CAPES, FINEP and EMBRACO. The authors would like to express their gratitude to their colleague Professor César Deschamps and former and present students Adriano da Silva, Antônio Lückmann, Fernando Grando, Huang Chieh, Marcus Alves, Moisés Marcelino-Neto, Murilo Ortolan, Paulo Couto, Rodrigo Kremer, Rodrigo Pizarro-Recabarren, Stefan Thoma and Tobias Gessner.

REFERENCES

[1] Coulomb D., Refrigeration: The challenges associated with sustainable development, *Proceedings of the 6th International Conference on Compressors and Coolants, Slovak Republic,* 2006, CD-ROM.

[2] Flohr F., Schwiegel M., and Meurer, C., Responsible refrigeration, *Proceedings of the 5th International Conference on Compressors and Coolants, Slovak Republic*, 2004, pp. 90-98.

[3] Trott A.R., and Welch T., *Refrigeration and Air-Conditioning*, 3rd Edition, 2000, Butterworth-Heinemann, UK

[4] Billiard, F., Refrigerating equipment, energy efficiency and refrigerants, *Proceedings of the 5th International Conference on Compressors and Coolants, Slovak Republic,* 2004, pp. 36-43.

[5] Gosney, W.B., *Principles of Refrigeration*, 1982, Cambridge University Press, UK.

[6] O`Neil, P.A., *Industrial Compressors*, 1993, Butterworth-Heinemann, UK

[7] Wang, S.K., *Handbook of air conditioning and refrigeration*, 2nd Edition, 2000, McGraw-Hill, NY.

[8] Possamai, F.C., and Todescat, M.L., A review of household compressor energy performance, *Proceedings of the 17th International Compressor Engineering Conference at Purdue,* 2004, paper C067.

[9] Pérez-Segarra, C.D., Rigola, J., Sòria, M., and Oliva, A., Detailed thermodynamic characterization of hermetic reciprocating compressors, *International Journal of Refrigeration*, vol. 28, pp. 579-593.

[10] Watson, M.C, Thermodynamics and heat transfer: Lubrication, *Proceedings of the Centenary Conference of the Institute of Refrigeration, London,* 1999, IMechE, UK.

[11] Cavestri, R.C., Measurement of viscosity, density and gas solubility of refrigerant blends in selected synthetic lubricants, Final Report, *Air-Conditioning and Refrigeration Technology Institute*, 1995.

[12] Mermond, Y., Feidt, M., Marvillet, C., Propriétés thermodynamiques et physiques des mélanges de fluides frigorigènes et d'huiles. *International Journal of Refrigeration*, vol. 22, 1999, pp. 569-579.

[13] Marsh, K.N., and Kandil, M.E., Review of thermodynamic properties of refrigerants + lubricant oils, *Fluid Phase Equilibria*, vol. 199, 2002, pp. 319-334.

[14] Pettersen, J., Carbon dioxide (CO_2) as a primary refrigerant, *Proceedings of the Centenary Conference of the Institute of Refrigeration, London,* 1999, IMechE, UK.

[15] Hauk, A. E., and Weidner, E., Thermodynamics and fluid-dynamic properties of carbon dioxide with different lubricants in cooling circuits for automobile application. *Industrial and Engineering Chemistry Research*, vol. 39, 2000, pp. 4646-4651.

[16] Tsuji, T., Tanaka, S., Hiaki, T., and Saito, R., Measurements of bubble point pressure for CO_2 + decane and CO_2 + lubricating oil. *Fluid Phase Equilibria*, vol. 219, 2004, pp. 87-92.

[17] Bobbo, S., Scattolini, M., Camporese, R., Fedele, L., and Stryjek, R., Solubility of carbon dioxide in some commercial POE oils. *Proceedings of the 7th IIR Gustav Lorentz Conference on Natural Working Fluids, Norway*, 2006, pp. 409-411.

[18] Seeton, C.J., and Hrnjak, P., Thermophysical properties of CO2-lubricant mixtures and their affect on 2-phase flow in small channels (less than 1 mm), *Proceedings of the 18th International Refrigeration and Air Conditioning Conference at Purdue*, 2006, Paper R170.

[19] Ancherbak, S.N., Semenyuk, Y.V., Skripov, P.V., and Zhelezny, V.P., An experimental investigation and modelling of the thermodynamic properties of R-245fa/compressor oil solutions, *Proceedings of the 6th International Conference on Compressors and Coolants, Slovak Republic,* 2006, CD-ROM.

[20] P.V. Zhelezny, V.P. Zhelezny, D.A. Procenko, S.N. Ancherbak, An experimental investigation and modeling of the thermodynamic properties of isobutane – compressor oil solutions: Some aspects of experimental methodology, *International Journal of Refrigeration*, vol. 30, 2007, pp. 433-445.

[21] Marcelino Neto, M.A., and Barbosa Jr., J.R., Solubility, density and viscosity of a mixture of R-600a and polyol ester oil, Submitted for publication, *International Journal of Refrigeration*.

[22] Marcelino Neto, M.A., and Barbosa Jr., J.R., Solubility and density of mixtures of R-744 and two synthetic lubricant oils, Submitted for publication, *Proceedings of the International Congress of Refrigeration, China*, 2007.

[23] Tesser, R., Musso, E., Di Serio, M., Basile, G., and Santacesaria, E., Description of the vapor-liquid equilibrium in binary refrigerant/lubricating oil systems by means of an extended Flory-Huggins model, *Journal of Fluorine Chemistry*, vol. 99, 1999, pp. 29-36.

[24] Grunberg, L., and Nissan, A.H., Mixture law for viscosity, *Nature*, vol. 164, 1949, pp. 799-800.

[25] Katti, P.K., and Chaudry, M.M., Viscosities of binary mixtures of benzil acetate with dioxane, aniline and m-cresol, *Journal of Chemical Data*, vol. 9, 1964, pp. 442-443.

[26] Fukuta, M., Yanagizawa, T., Shimizu, T., and Nishijima, H., Transient mixing characteristics of refrigerant with refrigeration oil, *Proceedings of the 19th International Congress of Refrigeration Iva*, 1995, pp. 215-222.

[27] Goswami, D.Y., Shah, D.O., Jotshi, C.K., Bhagwat, S.S., Leung, M., Gregory, A.S., and Lu S., Foaming characteristics of refrigerant/lubricant mixtures, *ARTI-MCLR Report* 665-53200, 1998.

[28] Yokozeki, A., Time-dependent behavior of gas absorption in lubricant oil, *International Journal of Refrigeration*, vol. 25, 2002, pp. 695-704.

[29] Fukuta, M., Yanagisawa, T., Omura, M. and Ogi, Y., Mixing and separation characteristics of isobutane with refrigeration oil, *International Journal of Refrigeration,* vol. 28, 2005, pp. 997-1005.

[30] Silva, A., Kinematics and dynamics of absorption of refrigerant in lubricant oil, D.Eng. Thesis (in Portuguese), Universidade Federal de Santa Catarina, Brazil, 2004.

[31] Prata, A.T, Grando, F.P., Silva, A., and Barbosa Jr., J.R., Improving compressor design through modeling of phase change and two-phase flow phenomena, *Proceedings of the 17th International Compressor Engineering Conference at Purdue,* 2004, paper C071.

[32] Gessner, T.R., and Barbosa Jr., J.R., Modeling absorption of pure refrigerants and refrigerant mixtures in lubricant oil, *International Journal of Refrigeration*, vol. 29, 2006, pp. 773-780.

[33] Taylor, R., and Krishna, R., *Multicomponent Mass Transfer*, Wiley, 1993.

[34] Toor, H.L., Diffusion in three component gas mixtures, *AIChE Journal*, vol. 3, 1957, pp. 198-207.

[35] Burton, C., Jacobi, A.M., and Mehendale, S.S., Vapor-liquid equilibrium for R-32 and R-410A mixed with a polyol ester: Non-ideality and local composition modeling, *International Journal of Refrigeration*, vol. 22, 1999, pp. 458-471.

[36] Barbosa Jr., J.R., and Ortolan, M.A., Experimental analysis of refrigerant mixing in lubricant oil, *Proceedings of the 6th International Conference on Compressors and Coolants, Slovak Republic,* CD-ROM., 2006.

[37] Barbosa Jr., J.R., and Ortolan, M.A., Experimental and theoretical analysis of refrigerant absorption in lubricant oil, Submitted for publication, *HVAC&R Research*.

[38] Barbosa Jr., J.R., Thoma, S., and Marcelino Neto, M.A., Behaviour of liquid temperature and onset of natural convection in refrigerant absorption in lubricant oil, To appear in *Proceedings of the 19th International Congress of Mechanical Engineering, Brasilia*, 2007.

[39] Tan, K.K., and Thorpe, R.B., The onset of convection caused by buoyancy during transient heat conduction in deep fluids, *Chemical Engineering Science*, vol. 51, 1996, pp. 4127-4136.

[40] Tan, K.K. and Thorpe, R.B., The onset of convection induced by buoyancy during gas diffusion in deep fluids, *Chemical Engineering Science*, vol. 54, 1999, pp. 4179-4187.

[41] Pizarro-Recabarren, R.A., Prata, A.T., and Barbosa Jr., J.R., A heat transfer analysis of the falling film oil flow on the inner shell of a hermetic reciprocating compressor, To be submitted.

[42] Incropera, F.P, and DeWitt, D.P., *Fundamentals of Heat and Mass Transfer*, 3rd Edition, Wiley, 1990, NY.

[43] Fagotti, F., Todescat, M.L., Ferreira, R.T.S., and Prata, A.T., Heat transfer modeling in reciprocating compressors, *Proceedings of the 12th Internatinal Compressor Engineering Conference at Purdue*, 1994, pp. 605-610.

[44] Kremer, R., Theoretical and Experimental Analysis of Oil Atomization in Compression Processes, M.Eng. Diss (in Portuguese), Universidade Federal de Santa Catarina, Brazil, 2006.

[45] Kremer, R., Barbosa Jr., J.R., and Deschamps, C.J., Theoretical analysis of the effect of oil atomization in the cylinder of a reciprocating compressor, To appear in *Proceedings of the International Conference on Compressors and their Systems, London, 2007.*

[46] Ussyk, M.S., Numerical simulation of hermetic reciprocating compressors, M.Eng. Diss., 1984, Federal University of Santa Catarina (in Portuguese).

[47] Bernardi, J.D., CFD simulation of a scroll compressor oil pumping system, *Proceedings of the 15th International Compressor Engineering Conference at Purdue,* pp 707-714, 2000.

[48] Cho, H., Yoo, B., Kim, Y., Chung, J.T., CFD simulation on the oil pump system of a variable speed scroll compressor, *Proceedings of the 16th International Compressor Engineering Conference at Purdue*, C24-1, CD-ROM, 2002.

[49] Kim, H.J., Lancey, T.W., Numerical study on the lubrication oil distribution in a refrigeration rotary compressor, *International Journal of Refrigeration*, vol. 26, pp. 800-808, 2003.
[50] Cui, M., Investigation on the oil supply system of a scroll compressor, *Proceedings of the 17th International Compressor Engineering Conference at Purdue*, C93, CD-ROM, 2004.
[51] Kim, H.J., Lubrication oil pumping by utilizing vane motion in a horizontal rotary compressor, *International Journal of Refrigeration*, vol. 28, pp. 498-505, 2004.
[52] Lückmann, A.J., Ribeiro, G.B., Danker, J.L., Barbosa Jr., J.R., Comparative Analysis of Comercial CFD Codes (CFX and FLUENT), Scientific Initiation Report (in Portuguese), Cooperation UFSC-EMBRACO, 2005.
[53] Asanuma M., ltami T., lshikawa H., An experimental study of the shaft oil supply mechanism of a rotary compressor, B, *Proceedings of the Compressor Engineering Conference at Purdue,* pp. 383-390, 1984.
[54] Drost, R.T., Quessada, J.F., Analytical and experimental investigation of a scroll compressor lubrication system, *Proceedings of the Compressor Engineering Conference at Purdue*, pp 551-560, 1992.
[55] ltho T., Kobayashi H., Fujitani M. Murata N., Study on the oil supply system, for rotary compressors, *Proceedings of the Compressor Engineering Conference at Purdue*, pp. 505-514, 1992.
[56] Alves, M.C., Barbosa Jr., J.R. and Prata, A.T., Analysis and simulation of the pumping oil flow for lubrication of hermetic reciprocating ccompressors, To be submitted.
[57] Huang, C., Couto, P.R.C. and and Prata, A.T., An integral analysis and simulation of the complete bearing system in reciprocationg hermetic compressors. To appear in *Proceedings of the International Conference on Compressors and their Systems, London, 2007*.
[58] Hamrock, B. J, Schmid, S. R. and Jacobson, B. O., *Fundamentals of Fluid Film Lubrication*, 2nd. edition, Marcel Dekker, 2004.
[59] Szeri, A. Z., *Fluid Film Lubrication - Theory & Design*, Cambridge University Press, 1998.
[60] Nakada, T., Yamamoto, A. and Abe, T. A Numerical approach for piston secondary motion analysis and its application to the piston related noise, SAE Paper No. 972043, 1997.
[61] Prata, A.T., Fernando J.R.S. and Fagotti, F., Dynamic analysis of piston secondary motion for small reciprocating compressors, *Journal of Tribology*, vol. 122, pp. 752-760, 2000.
[62] Rigola, J., Perez-Segarra, C.D., and Oliva, A., Numerical simulation of the leakage through the radial clearance between piston and cylinder in hermetic reciprocating compressors, *Proceedings of the International Conference of Compressors and their Systems*, London, UK, pp. 313–321, 2003.
[63] Kim, T.J. and Han, J.S, Comparison of the dynamic behaviour and lubrication characteristics of a reciprocating compressor crankshaft in both finite and short bearing models, *Tribology Transactions*, vol. 47, pp. 61-69, 2004.
[64] Cho, J.R. and Moon, S.J., A numerical analysis of the interaction between the piston oil film and the component deformation in a reciprocating compressor, *Tribology International*, vol. 38, pp. 459–468, 2005.
[65] Grando, F.P., Priest, M. and Prata, A.T., Lubrication in refrigeration systems: numerical model for piston dynamics considering oil–refrigerant interaction, *Journal Engineering Tribology*, vol. 220, pp. 245-258, 2006.
[66] Chieh, H., Modeling and Computational Analysis of Shaft, Connecting Rod and Piston Lubrication in Reciprocating Compressors, M.Eng. Diss (in Portuguese), Universidade Federal de Santa Catarina, Brazil, 2007.
[67] Couto, P.R.C., Analysis of Hydrodynamic Radial Bearings with Application in Refrigeration Hermitic Compressors, D.Eng. Thesis (in Portuguese), Universidade Federal de Santa Catarina, Brazil, 2006.
[68] Grando, F.P., Priest, M. and Prata, A.T., A two-phase flow approach to cavitation modelling in journal bearings, *Tribology Letters*, vol. 21, pp. 233-244, 2006.
[69] Dowson, D. and Taylor, C.M., Cavitation in Bearings, Annual Review of Fluid Mechanics, vol. 11, pp. 35-66, 1979.